# Semiconductor Laser Insert with Uniform Illumination for Use in Photodynamic Therapy

*Ivan Charamisinau*[*], *Gemunu Happawana*[*], *Gary Evans*[**],

*Arye Rosen*[+] *Richard A. Hsi*[++] *and David Bour*[+++]

** Department of Mechanical Engineering, Southern Methodist University, Dallas, TX 75275*

*Phone (214)768-1966, E-mail: icharami@engr.smu.edu*

[**] *Department of Electrical Engineering, Southern Methodist University, Dallas, TX 75275*

[+]*School of Biomedical and Electrical Engineering, Drexel University, Philadelphia, PA 19104*

[++]*Department of Radiation Oncology, Hospital of the University of Pennsylvania, Philadelphia, PA 19104*

[+++]*Agilent Technologies, dave_bour@exeh.labs.agilent.com*

**Key words:** 140.5960 Semiconductor Lasers, 170.5180 Photodynamic therapy, 220.4830 Optical systems design, 290.4020 Mie theory, 290.5850 Scattering, Particles, 290.5850 Scattering, rough surfaces.

**Abstract:** A low cost semiconductor red laser light delivery system for esophagus cancer treatment is presented. The system is small enough for insertion into the patient's body. Scattering elements with nanoscale particles are used to achieve uniform illumination. The scattering element optimization calculations, using Mie theory, provide scattering and absorption efficiency factors for scattering particles composed of various materials. The possibility of using randomly deformed spheres and composite particles instead of perfect spheres is analyzed using an extension to Mie theory. The measured radiation pattern from a prototype light delivery system fabricated using the design criteria in this paper shows reasonable agreement with the theoretically predicted pattern.

# 1.Introduction

Photodynamic therapy (PDT) is a promising method of cancer treatment[1-3] with minimal side effects. It uses a photosynthesizing drug (typically porfimer sodium) that becomes toxic after it is activated by 635 nm red light. The drug is administered to the patient 10-48 hours before treatment[4]. During that time the drug accumulates mainly in cancerous cells. The 635 nm red light illuminates the cancerous area activating the drug to destroy the cancerous cells without damaging surrounding healthy tissue and without the cumulative toxicity associated with ionizing radiation.

PDT using Photofrin has been approved by the U.S. Food and Drug Administration (FDA) and has successfully treated almost all cancers, including breast, bladder, colon, esophageal, gynecologic, head, lung, neck, prostate, and skin cancer. PDT also provides an option for treatment for patients who have not met with success with the usual approaches of surgery or chemotherapy and is easy on the patient – unlike other cancer treatments.

The purpose of lasers in PDT is to initiate photochemical reactions in contradistinction to their photothermal or photomechanical effects as seen in other treatment techniques[5]. Lasers are used as a light source because of their monochromaticity that provides maximum effectiveness if the wavelength of the laser corresponds with the peak absorption of the photosensitizer. Also lasers can produce high irradiance to minimize the therapeutic exposure time and can be readily coupled to fiber optics, enabling light delivery to any organ, such as the bladder, gastrointestinal tract, or lungs.

Initial PDT systems used large, expensive gold vapor lasers, tunable dye lasers pumped by argon ion, copper vapor, frequency-doubled Nd:YAG, potassium-titanyl-phosphate (KTP/YAG), or excimer lasers. These lasers are large, often water-cooled, require three-phase power, specialized facilities, special maintenance, and have high initial as well as operating costs. During the last decade PDT systems based on coupling semiconductor lasers[6] or LEDs to fibers have become available.

Usually fibers with light diffusing sections[7,8] are used to achieve uniform lighting. A concept for embedding LEDs in tumors has also been patented[9]. Another alternative is the use of diode lasers directly in a balloon catheter as shown in Fig. 1. These semiconductor laser systems can simultaneously accommodate multiple wavelengths as newer photosensitizing drugs become available which may be activated at different wavelengths.

## 2. System Design

A new design of a portable and inexpensive light delivery system for esophagus cancer treatment that uses tiny semiconductor lasers placed in a balloon catheter, which is inserted directly into the esophagus is proposed. This approach avoids power losses in coupling the laser to the fiber and reduces the system size while increasing reliability and efficiency. Additionally, different groups of lasers can be turned on and off to vary the illuminated area.

The laser packaging problems that arise are: (1) the balloon catheter with the lasers must be flexible and must have a small diameter, (2) the lasers must be at a uniform, fixed temperature to maintain the emission wavelength, and (3) the lasers require a scattering element to achieve uniform illumination.

The PDT of Barrett's esophagus requires a light delivery system with the following specifications: (1) emission at a wavelength of 635±2 nm, (2) a total output power of 4 W, (3) uniform light distribution over about 10 cm of esophagus, and (4) a deflated balloon catheter outer diameter of less than 10 mm.

The balloon catheter (shown in Fig. 1) uniformly distributes light radially from 21 red lasers over a length of 10 cm. The proposed concept uses active water-cooling to extract the heat generated by the lasers. The lasers are mounted on submounts to spread the heat and the submounts are mounted on copper cooling tubes, as shown in Fig. 2b. The inner diameter of the laser insert is 8.5 mm. To achieve the required flexibility, the sections of the copper tubes are separated by sections of flexible plastic tubing, as

shown in Fig. 2a. The triangular arrangement shown in Fig. 2b allows maximum space for cooling while minimizing shadows. The optical output power can be increased by adding more lasers.

## 3. Laser Structure

For most telecommunications applications laser structures are optimized to have a small beam divergence to efficiently couple light into a fiber. For the PDT application, this constraint does not exist and the epitaxial structure of the semiconductor laser can be optimized to achieve improved efficiency and larger beam divergences. We have used WAVEGUIDE[13] to model AlGaInP/GaAs 635 nm lasers[14] and have determined the optimal layer compositions and thicknesses to achieve maximum efficiency. The resulting beam divergence from the laser is ~ 45°.

## 4. Optical Scattering Element

To achieve uniform illumination of the esophagus, optical scattering elements on both laser facets are necessary. The light entering these scattering elements will be scattered in random directions by small particles in a light-transparent polymer media resulting in uniform lighting. The amount of light scattering polymer required is a trade-off between uniformity and absorption. The optimum polymer thickness can be found by determining the dependence of the scattered far field on the amount of polymer, on the density and on the size of the particles in the polymer. Uniform illumination with a minimum loss of irradiated power is desired. The proposed scattering polymer element on the laser facets eliminates the need for using higher loss lipids as the scattering media[15].

Polymer scattering elements are deposited on both facets of the laser chip as shown in Fig. 2c. Increased light uniformity and increased absorption occurs with increasing scattering element size. The optimum choice for the thickness of the polymer scattering element depends on the far field of the laser and on the density and size of the particles in the polymer

Consider a rectangular piece of polymer material with width a, height b and length L containing N scattering particles as shown in Fig. 3.

The effectiveness of scattering photons traveling along the z axis is given by the efficiency factor[16] $Q_{sca} = C_{sca}/G$ where $C_{sca}$ is the cross sectional area that intercepts the same light intensity as is scattered by a particle of cross section $G$. $Q_{sca}$ is found by integrating the scattering intensity function $F(\theta,\varphi)$[16]:

$$Q_{sca} = \frac{1}{k^2 G}\int_0^{\pi}\int_0^{2\pi} F(\theta,\varphi)\sin(\theta)\,d\varphi\,d\theta \tag{1}$$

where $r$, $\theta$, $\varphi$ are spherical coordinates, $k = 2\pi m_p/\lambda$ is the wave vector in the polymer, $m_p$ is the refractive index of the polymer and $\lambda$ is the free-space wavelength.

Similarly, the effectiveness of absorbing such photons is given by the efficiency factor $Q_{abs}=C_{abs}/G$ and the effectiveness of extinction of the photons along the x direction (which is the sum of absorption and scattering) is given by the efficiency factor $Q_{ext}=C_{ext}/G = Q_{sca}+Q_{abs}$. $C_{abs}$ is the cross sectional area that intercepts the same light intensity as is absorbed by a particle of cross section $G$ and $C_{ext}$ is the area that intercepts the same light intensity as is attenuated by a particle of size $G$.

Expressions for $Q_{ext}$ and $Q_{abs}$ are given in Section 5 for spherical particles, in Section 7 for deformed spheres and in Section 8 for composite spheres.

The scattering efficiency defined in Eq. (1) is an average of the scattering intensity function. However, in many cases (especially for big particles) most light is scattered within a very small angle as depicted in Fig. 4. Such low angle scattering contributes to the attenuated far-field radiation pattern of the laser shown in Fig. 5a. The intensity of the large angle scattering is nearly uniform, so an efficiency factor for large angular scattering can be defined by:

$$Q_{scu} = \frac{\sqrt{2}}{k^2 G}\int_{\pi/4}^{3\pi/4}\int_0^{2\pi} F(\theta,\varphi)\sin(\theta)\,d\varphi\,d\theta \tag{2}$$

As illustrated in Fig. 4 for a silver sphere, the large angle scattering intensity is nearly uniform resulting in a uniform background contribution to the angular far-field (Fig. 5b). For this reason, the integration over $\theta$ in Eq. (2) is insensitive to the limits of integration if $\theta$ is outside the low-angle scattering limit.

From geometrical considerations, the probability $p$ of scattering a photon from a sphere of diameter $D$ is:

$$p = \frac{GQ_{scu}}{a^2} = \frac{\pi D^2 Q_{scu}(D)}{4a^2} \tag{3}$$

The probability that the photon will pass through a polymer containing $N$ particles without scattering is:

$$T = (1-p)^N. \tag{4}$$

Assuming a large number ($N$>>1) of small particles ($p$<<1), Eq. (4) becomes:

$$T = \exp(-pN) = \exp\left[-\frac{\pi D^2 Q_{scu}(D)}{4a^2}\frac{6P_g a^2 L}{\pi D^3}\right] = \exp\left[-\frac{3P_g L Q_{scu}(D)}{2D}\right] \tag{5}$$

where $P_g$ is the fraction of particles by volume in the polymer ($P_g = \pi D^3 N/(6a^2 L)$).

Equation (5) indicates that $T$ does not depend on the cross-sectional area or the shape of the polymer material but only on the distance that light travels in the light-scattering media. $T$ is also the percentage of light that passes through the media without scattering.

A metric for the far-field uniformity from the scattering element (Fig. 5c) is the fringe visibility $V$ defined by $(I_{max}-I_{min})/I_{max}$. For PDT applications, a fringe visibility of 0.5 provides reasonable uniformity.

If the laser power is equal to $P$ then the total scattered light power is $P(1-T)$ and total transmitted power is $PT$. The scattered light (Fig. 5b) is uniformly distributed over the $\pi/2$ radians indicated in Fig. 2c and has intensity (shown in Fig. 5c)

$$I_{min} = P(1-T)2/\pi \tag{6}$$

A Gaussian distribution is assumed for the transmitted light:

$$I_{tr}(\theta) = PT\frac{2}{\sqrt{2\pi}}\frac{2}{0.849\theta}\exp\left(\frac{-\theta^2}{2\Delta\theta^2}\right) \tag{7}$$

where $\Delta\theta$ is the full width at half power (FWHP) of the far-field of the laser without a scattering element. From Eq. (7) the maximum intensity of the far field (see Fig. 5c) is:

$$I_{max} = I_{min} + PT4/(0.849\theta\sqrt{2\pi}), \tag{8}$$

and the visibility $V$ is given by:

$$V = 1 - \frac{I_{\min}}{I_{\max}} = 1 - \left[ P(1-T)\frac{2}{\pi} \right] \Big/ \left[ P(1-T)\frac{2}{\pi} + PT\frac{2}{\sqrt{2\pi}}\frac{2}{0.849\theta} \right]. \quad (9)$$

By solving equation (9) for $T$:

$$T = \left[ 1 + \frac{(1-V)\sqrt{2\pi}}{0.849\theta V} \right]^{-1}. \quad (10)$$

For $V$ =0.5 and $\theta$=45° we find that $T$ is equal to 0.21.

From Eq. (5) we can find the length $L$ required for a given amount of transmission, $T$:

$$L = \frac{-2D\ln(T)}{3P_g Q_{scu}(D)}. \quad (11)$$

The scattering element will be most efficient when the value of $Q_{scu}(D)/D$ is maximum. Generally the particle size and spacing determines the type of light scattering and which theory should be used for scattering calculations:

1. Geometrical optics is valid when $D$ > (3-6)$\lambda$, ($D$ > 2-4 μm for $\lambda$ = 635 nm) and $D(m-1)$ is big, where λ is the wavelength of the scattered light and m is the refractive index of the particle.
2. Rayleigh Scattering is valid when $D$ < (0.05-0.1)$\lambda$, ($D$ < 30-50 nm for $\lambda$ = 635 nm) and $Dm$ is small
3. Mie scattering is used when (0.05 - 0.1)$\lambda$ < $D$ < (3-6)$\lambda$.

For geometrical optics (big particles, $D >> \lambda$), $Q_{scu}(D)$ = 1 because diffraction effects are negligible and $Q_{sca}(D)$ = 2, due to the extinction partadox[16]. Since $L \sim D/Q_{scu}$, for the geometrical case smaller particles are desired.

For Rayleigh scattering ($D << \lambda$), $Q_{scu}(D) \approx Q_{sca}(D) \sim D^4$, so $L \sim D^{-3}$, so in this case, bigger particles are desired.

From these Rayleigh and geometrical considerations, the optimum particle size is in the range treated by Mie theory. Mie theory is applicable to sparsely spaced particles, or equivalently when every particle is in the far-field of the light scattered by the other particles (which corresponds to a spacing of > 3$\lambda$). This requirement limits the volume fraction of 0.45 μm particles in a polymer to about 1%, and limits the

volume fraction of particles for 0.12 μm particles to about 0.1%. For more closely spaced particles we would need to apply Maxwell's equations to the ensemble of particles.

## 5. Mie Theory for Light Scattering on Spheres

The scattered wave from a particle using Mie theory is described by functions u and v[16]:

$$u = e^{i\omega t}\cos\varphi\sum_{n=1}^{\infty} -a_n(-i)^n\frac{2n+1}{n(n+1)}P_n^1(\cos\theta)h_n^{(2)}(kr) \tag{12a}$$

$$v = e^{i\omega t}\sin\varphi\sum_{n=1}^{\infty} -b_n(-i)^n\frac{2n+1}{n(n+1)}P_n^1(\cos\theta)h_n^{(2)}(kr) \tag{12b}$$

where $r$, $\theta$ and $\varphi$ are spherical coordinates, ω is the oscillation frequency, $i$ is $\sqrt{-1}$, $P_n^1(x)$ are Legendre polynomials, $a_n$ and $b_n$ are coefficients that represent mode amplitudes, $h_n^{(2)}(x)$ are spherical Bessel functions derived from the second kind of Bessel functions.

The functions $u$ and $v$ are related to the field components by[16]:

$$\mathbf{E} = \nabla\times(\mathbf{r}v) + (i/mk)\nabla\times\nabla\times(\mathbf{r}u)\,, \tag{13a}$$

$$\mathbf{H} = m[\,-\nabla\times(\mathbf{r}u) + (i/mk)\nabla\times\nabla\times(\mathbf{r}v)\,]\,, \tag{13b}$$

where **E** is the electric field, **H** is the magnetic field, **r** is the coordinate vector, $m$ is the complex refractive index of the media.

The coefficients $a_n$ and $b_n$ are found from boundary conditions[16]:

$$a_n = \frac{\psi'_n(y)\psi_n(x) - m\psi_n(y)\psi'_n(x)}{\psi'_n(y)\zeta_n(x) - m\psi_n(y)\zeta'_n(x)}\,, \qquad b_n = \frac{m\psi'_n(y)\psi_n(x) - \psi_n(y)\psi'_n(x)}{m\psi'_n(y)\zeta_n(x) - \psi_n(y)\zeta'_n(x)} \tag{14}$$

where $\psi_n(x)$ and $\zeta_n(x)$ are related to the Bessel functions:

$$\psi(z) = \sqrt{\pi z/2}J_{n+1/2}(z), \qquad \chi(z) = -\sqrt{\pi z/2}N_{n+1/2}(z), \qquad \zeta(z) = \sqrt{\pi z/2}H^{(2)}_{n+1/2}(z) \tag{15}$$

and the arguments $x$ and $y$ are defined as:

$$x = ka = kD/2 = \frac{\pi D}{\lambda}, \tag{16a}$$

$$y = mka = \frac{m\pi D}{\lambda} \tag{16b}$$

The scattering intensity function $F(\theta,\varphi)$ is[16]:

$$F(\theta,\varphi) = \left|S_2^2(\theta)\right|\cos^2\varphi + \left|S_1^2(\theta)\right|\sin^2\varphi\,, \tag{17a}$$

where

$$S_1(\theta) = \sum_{n=1}^{\infty}\frac{2n+1}{n(n+1)}\left[a_n\pi_n(\cos\theta) + b_n\tau_n(\cos\theta)\right], \tag{17b}$$

$$S_2(\theta) = \sum_{n=1}^{\infty}\frac{2n+1}{n(n+1)}\left[b_n\pi_n(\cos\theta) + a_n\tau_n(\cos\theta)\right], \tag{17c}$$

$$\pi_n(\cos\theta) = \frac{1}{\sin\theta}P_n^1(\cos\theta)\,, \tag{17d}$$

$$\tau_n(\cos\theta) = \frac{d}{d\theta}P_n^1(\cos\theta) \tag{17e}$$

The efficiency factor for extinction[16] is found from either Eq. (17b) or (17c) for $\theta = 0$:

$$Q_{ext} = \frac{4}{x^2}\mathrm{Re}[S_1(0)] = \frac{4}{x^2}\mathrm{Re}[S_2(0)] = \frac{2}{x^2}\sum_{n=1}^{\infty}(2n+1)\,\mathrm{Re}(b_n + a_n) \tag{18}$$

Using Eq (17a) in Eq. (1) and integrating with respect to $\theta$ and $\varphi$ gives the scattering efficiency:

$$Q_{sca} = \frac{1}{x^2}\int_0^{\pi}\left[\left|S_1^2(\theta)\right| + \left|S_2^2(\theta)\right|\right]\sin\theta d\theta \tag{19}$$

Equation (19) can be reduced to[17]:

$$Q_{sca} = \frac{2}{x^2}\sum_{n=1}^{\infty}(2n+1)[|a_n|^2 + |b_n|^2] \tag{20}$$

Using Eqs. (18) and (20), we can find absorption efficiency factor:

$$Q_{abs} = Q_{ext} - Q_{sca} \tag{21}$$

The uniform scattering efficiency factor is found by using Eq. (17a) in Eq. (2) and integrating with respect to $\theta$ and $\varphi$:

$$Q_{scu} = \frac{\sqrt{2}}{x^2}\int_{\pi/4}^{3\pi/4}\left[\left|S_1^2(\theta)\right| + \left|S_2^2(\theta)\right|\right]\sin\theta d\theta \tag{22}$$

## 6. Optimization of Particle Size for Highest Scattering and Lowest Absorption

Mie theory simulation software developed at SMU was used to find the best material and the optimum particle size for the polymer scattering material. The scattering element was optimized to give the highest scattering with the smallest size. The scattering element size can be found from Eq. (11) and is

governed by the factor $Q_{sca}(D)/D$. Loss from an ensemble of particles is obtained by replacing $T$ by 1 - $A_p$ and inserting $Q_{abs}$ in the exponential term:

$$1 - A_p = \exp(-\frac{3P_g Q_{abs}}{2D} L), \tag{23}$$

where $A_p$ is the fraction of light absorbed by the particles in the scattering element. If we also consider the loss due to absorption by the polymer in the scattering elements, we find:

$$1 - A = \exp(-\frac{3P_g Q_{abs}}{2D} L)\exp(-\alpha_m L) \tag{24}$$

where $\alpha_m$ is the loss in the polymer material, $A$ – total loss in the polymer, $A=(P_{in}-P_{out})/P_{in}$, $P_{in}$ is the optical power produced by laser diode, $P_{out}$ is the optical power that comes out of the scattering element.

If we substitute $L$ from Eq. (11) in Eq. (24) we get

$$1 - A = \exp\left[\left(\frac{Q_{abs}}{Q_{scu}} + \frac{\alpha_m 2D}{3P_g Q_{scu}}\right)\ln T\right] \tag{25}$$

Since $T$ is less than 1, for maximum transmission we want the terms in parentheses that multiply lnT to be small. For metal scattering particles in the scattering element, the ratio of $Q_{abs}/Q_{scu}$ is in the range of 0.03 to 3.0 and $\alpha_m$ is small (5x10-6 micron$^{-1}$) so the term it multiples can be neglected for practical values of $P_g$, $D$ and $Q_{scu}$. For light transparent scattering particles the imaginary part of the refractive index is small, so the $Q_{abs}/Q_{scu}$ term in Eq. (25) is small and can be neglected compared to the polymer loss term.

Figure 6 shows the absorption and scattering efficiencies for silver and gold. Although gold has the highest scattering and highest absorption efficiency at a normalized particle size of 0.7, the optimum ratio of $Q_{abs}/Q_{scu}$ for gold is 6.73 and occurs at a particle size of 0.12 μm, as listed in Table 2. Similarly, the optimum ratio of $Q_{abs}/Q_{scu}$ for silver is 22.6 and occurs at a particle size of 0.1 μm, indicating that silver is the best choice for a metal particle scatterer.

Equation (25) was used to generate the data for scattering and absorption efficiencies for single particles to generate the scattering element parameters shown in Table 2. The smallest scattering element size, about 1 μm, is achieved for metal scattering particles with diameters in of ~ 0.05 μm as shown in

Fig. 7. To avoid the rapid increase in loss that occurs for particle diameters of less than ~ 0.05 μm, diameters of > 0.1 μm are chosen.

Using is 0.1 μm diameter silver particles, uniform illumination can be achieved with a 3.6 μm thick scattering element with 7% absorption. The scattering element size can be increased by reducing the particle density.

The processes that take place at each particle can be understood by considering the efficiency factors. For example the 0.12 micron gold particle (see Table 1) distorts 5 times ($Q_{ext} \approx 5$) more light than it intercepts or in other words it distort as much light as 0.27-micron particle would in geometrical optics. Out of all the distorted optical energy, 70% is scattered uniformly ($Q_{scu}/Q_{ext} \approx 0.7$), 20% is low-angular scattering ($(Q_{sca}-Q_{scu})/Q_{ext} \approx 0.2$ ) and 10% is absorbed ($Q_{abs}/Q_{ext} \approx 0.1$).

Light transparent particles such as glass can be used for scattering particles in the scattering elements. Such particles have negligible absorption, more than 6 orders of magnitude less than for metals. Because of the low scattering efficiency, the size of the scattering element is larger. As an example, Table 2 shows that a scattering element with 0.15 μm glass particles will be 280 μm thick.

The performance and size of scattering elements with light transparent particles is determined by the real part of the refractive index of the particle. Figure 8 shows that a reasonable scattering element size below 100 micron can be achieved for light transparent particles with refractive indices either below 1.2 or over 1.8.

The total loss in the scattering element and the scattering element size for scattering particles made of any material with arbitrary complex refractive index can be found from Fig. 9. The materials that simultaneously are in the darker regions in both Fig. 9a and Fig. 9b are most suitable for scattering element fabrication. This is because the darker regions of Fig. 9a have lower scattering element loss and the darker regions of Fig. 9b have smaller scattering element size. If the scattering element absorbs less than 10% of the light, it is labeled "good" in Fig. 9a. Similarly, the inner diameter of laser insert limits the scattering element about one-half millimeter or less, so scattering elements smaller than 0.5 mm are

considered "good" in Fig. 9b.

## 7. Particles with Deformed Shapes.

The scattering calculations above were made for spherical particles. If the particle is not spherical, it can be modeled by using a variable radius:

$$r(\theta,\phi) = r_0 + \Delta r \sin(K\theta) \sin(K\phi), \tag{26}$$

where $r_0$ is the mean radius, $\Delta r$ is the variation of the radius, and $K$ is the shape parameter.

The scattering and absorption efficiency factors for such rough-shaped particles can be calculated by finding the modes of the particle and matching the incident field through the boundary conditions at the surface given by Eq. (26) to those modes. Although the most general case is complicated, we can simplify the problem assuming 'smooth roughness' (small $K$ and $\Delta r/r_0$). This assumption allows neglecting $\theta$ and $\varphi$ components of the normal vector **n** in the boundary conditions and use of the same equations for modes inside and outside the particle. The diameter $D$ in Eq. (16) is determined by Eq. (26) and is no longer a constant. The boundary conditions are found using Eq. (14) but with x, y, $a_n$ and $b_n$ depending on $\theta$ and $\varphi$. The scattering intensity function, $Q_{ext}$, $Q_{sca}$ and $Q_{abs}$ (Eqs. 17, 18, 20, 21) also must be evaluated with $x$, $y$, $a_n$ and $b_n$ depending on $\theta$ and $\varphi$.

Finally, the scattering efficiency factor is found from:

$$Q_{scu} = \frac{1}{\sqrt{2}\pi x^2} \int_{\pi/4}^{3\pi/4} \int_{0}^{2\pi} \left[ \left| S_1^2(\theta,\varphi) \right| + \left| S_2^2(\theta,\varphi) \right| \right] d\varphi \sin\theta d\theta \tag{27}$$

Equation (27) is solved numerically using MathCAD. The scattering and absorption efficiency for a 1 micron gold particle are shown in Fig.11 as a function of particle roughness.

The results obtained by the method above are valid only as long as the assumption of smooth roughness is valid or when $n_\theta$ and $n_\varphi$ components of normal vector **n** are small. The radial component of the normal vector **n** averaged over particle surface is shown on Fig. 12. Clearly, the validity of the above method becomes questionable as $\Delta r/r_0$ is increases above 20%. The calculation of the absorption efficiency is numerically less accurate, since two large numbers (Eq. (21)) are being subtracted.

These results show that particles with slightly deformed shapes have somewhat better scattering performance than spherical particles.

## 8. Composite Particles

Composite core-shell nanoparticles[19,20] exhibit effects such as plasmon optical resonances and photonic band gaps that cause increased light extinction at certain wavelengths.

A composite particle can be modeled as two concentric spheres with a core and a shell, as shown in Fig. 13. The shell of the particle has a radius $r_0$ and the core has a radius $r_0 - \Delta r = r_0 (1 - \delta r)$.

The scattered wave $\Omega_1$ is found by considering an incident wave $\Omega_0$ and the waves transmitted into and reflected from the core ($\Omega_3$) and shell ($\Omega_2$), all of which can be expressed in terms of the scalar functions *u* and *v* as in the case of spherical particles (Eq. (12)).

Waves in the shell layer ($\Omega_2$) are represented by general solution with Bessel functions of both kinds[10]:

$$u = e^{i\omega t}\cos\varphi\sum_{n=1}^{\infty} m_2(-i)^n \frac{2n+1}{n(n+1)} P_n^1(\cos\theta)[c_n j_n(m_2 kr) - d_n n_n(m_2 kr)] \tag{28a}$$

$$v = e^{i\omega t}\sin\varphi\sum_{n=1}^{\infty} m_2(-i)^n \frac{2n+1}{n(n+1)} P_n^1(\cos\theta)[e_n j_n(m_2 kr) - f_n n_n(m_2 kr)] \tag{28b}$$

To find the field distributions in regions 1 (polymer), 2 (shell) and 3 (core), we need the coefficients $a_n$, $b_n$, $c_n$, $d_n$, $e_n$, $f_n$, $g_n$ and $h_n$ which are found from the boundary conditions. There are two boundaries (at the polymer-shell interface and at the shell-core interface) and we have 8 equations (both the **E** and **H** fields (or equivalently u and v) and their derivatives are continues at the boundaries) with 8 unknowns $a_n$, $b_n$, $c_n$, $d_n$, $e_n$, $f_n$, $g_n$ and $h_n$.

$$a_n = \frac{s_n \psi'_n(x_2) - \psi_n(x_2)}{s_n \zeta_n'(x_2) - \zeta_n(x_2)}, \tag{29a}$$

$$b_n = \frac{t_n \psi'_n(x_2) - \psi_n(x_2)}{t_n \zeta_n'(x_2) - \zeta_n(x_2)}, \tag{29b}$$

$$s_n = m_2 \frac{\psi_n(y_2) + p_n \chi_n(y_2)}{\psi'_n(y_2) + p_n \chi'_n(y_2)}, \tag{29c}$$

$$t_n = \frac{1}{m_2}\frac{\psi_n(y_2)+q_n\chi_n(y_2)}{\psi'_n(y_2)+q_n\chi'_n(y_2)}, \tag{29d}$$

$$p_n = \frac{d_n}{c_n} = \frac{m_2\psi'_n(y_3)\psi_n(x_3)-m_3\psi_n(y_3)\psi'_n(x_3)}{m_3\psi_n(y_3)\chi'_n(x_3)-m_2\psi'_n(y_3)\chi_n(x_3)}, \tag{29e}$$

$$q_n = \frac{f_n}{e_n} = \frac{m_3\psi'_n(y_3)\psi_n(x_3)-m_2\psi_n(y_3)\psi'_n(x_3)}{m_2\psi_n(y_3)\chi'_n(x_3)-m_3\psi'_n(y_3)\chi_n(x_3)}, \tag{29f}$$

$$c_n = \frac{\psi'_n(x_2)-a_n\zeta'_n(x_2)}{\psi'_n(y_2)+p_n\chi'_n(y_2)}, \tag{29g}$$

$$d_n = \frac{\psi_n(x_2)-b_n\zeta_n(x_2)}{\psi_n(y_2)+q_n\chi_n(y_2)}, \tag{29h}$$

$$g_n = \frac{c_n}{\psi'_n(y_3)}\left[\psi'_n(x_3)+p_n\chi'_n(x_3)\right], \tag{29i}$$

$$h_n = \frac{e_n}{\psi_n(y_3)}\left[\psi_n(x_3)+q_n\chi_n(x_3)\right]. \tag{29j}$$

Knowing $a_n$ and $b_n$ allows calculation of the efficiency factors $Q_{ext}$, $Q_{sca}$, $Q_{abs}$, $Q_{scu}$ using the same formulas we used for Eqs. (17), (18), (20), (21) and (22).

Computational difficulties with Eq (29), due to the possibility of near zero values in both the numerator and denominator, may be avoided by using 64-bit precision.

Modeling of composite particles show a very high extinction peak caused by increased absorption in the shell due to a resonance in the core. Figure 14 shows the results of calculations for a silver shell on a glass core. For a silver shell thickness that is 10% of the particle radius, the absorption increases 15 times compared to a pure silver particle of the same size, while the uniform scattering increases only 30%. Similar results were observed for other metals. Although metal shells on dielectric cores are not desirable for scattering elements, their enhanced absorption over solid metal shells make them ideal for insertion into tumors for increased absorption of radiation.

Composite particles with a metal core and a light transparent shell behave just like metal particles without any shell.

Dielectric composite particles, made of two different types of a light transparent dielectric can show enhanced scattering over a single dielectric scattering particle. Figure 15 shows the scattering

efficiency for a light transparent composite particle with a core refractive index of 1.65 and a shell refractive index of 1.33. The scattering efficiency of a particle with a shell thickness that is 40% of the total particle radius is 2.5 times higher than that of a spherical particle made of solid glass with an index of 1.33 or 1.65.

## 9. Scattering Element Design

From the figures and tables above, efficient scattering elements can be fabricated using either dielectric or metal particles with diameters of about 0.1 μm. Because of their greater scattering efficiency, smaller scattering elements can be made from metal particles, although the total loss is about 7%. Using metal particles at a wavelength of 635 nm, the best scattering element is made from a 1:100 volume ratio of 0.1 μm diameter silver particles mixed with a light transparent epoxy (with an index of 1.5). The size of this scattering element is ~ 4 μm and has a loss of ~ 7%. A scattering element of this size could be deposited as a thin film on the facet of a laser using sputtering or electron-beam deposition.

Using light transparent dielectric particles at a wavelength of 635 nm, the best scattering element is made from a 1:1000 volume ratio of 0.15 μm $TiO_2$ particles mixed with a light transparent epoxy (with an index of 1.5). The size of this scattering element is ~ 100 μm and has a loss of ~ 0.1%. Because of such low losses, the size of scattering elements using dielectric particles can be increased by even an order of magnitude, providing even more uniformity in the far-field. Microjet technology[21] is one method of producing larger (tens to thousands of microns) scattering elements on laser diodes in a controlled manner.

Scattering elements based on composite particles generally were less efficient than those based on all metal or all dielectric scattering particles. The exception is the use of composite particles made of a low-index outer shell and high-index light core, which are as efficient as, or slightly more efficient (as much as 5 to 10%) than uniform composition scattering particles. Although such composite scattering particles are about 3 times more effective at scattering light, their size is about 3 times larger, so by Eqs. (11) and (25), the efficiency of the composite based scattering element is about the same as a uniform

dielectric based scattering element.

An example of a composite based scattering element (at a wavelength of 635 nm) is a 1:1000 volume ratio of 0.45 μm particles (1.2 index shell, $TiO_2$ core) in a light transparent epoxy (with an index of 1.5). The size of this scattering element is ~ 200 μm and has a loss of ~ 0.1%.

## 10. Light Delivery System Radiation Pattern

The far field radiation pattern of the complete laser insert is determined by summing the contributions from the individual scattering element far fields (Fig. 5) which are configured as shown in Fig. 2.

Using cylindrical coordinates (φ, r, z), the radial far field on the surface of the esophagus (r = R = 10 mm) can be found from the geometry of Fig.16, ignoring the size of the laser (0.25 mm is negligible compared to 10 mm).

From basic trigonometry, θ, dθ and $R_1$ are given by

$$R_1 = \sqrt{R^2 + t^2 - 2tR\cos\varphi} \ , \tag{30a}$$

$$\theta = \arcsin\left(\frac{R^2 - t^2 - R_1^2}{2tR_1}\right) sign[\sin(\varphi)] + \frac{\pi}{2}\{1 - sign[\sin(\varphi)]\} \ , \tag{30b}$$

$$d\theta = \sin(\theta + \varphi)d\varphi \tag{30c}$$

The radial far field produced by a single facet of the laser can be approximated as a Gaussian (Eq. (7)) on a pedastal (Eq 6):

$$I_s(\varphi) = \frac{\sin(\theta + \varphi)d\varphi}{R_1^2}\left[\frac{1-T}{\pi} + \frac{T}{\sqrt{2\pi}\Delta\theta}\exp\left(-\frac{\theta^2}{2\Delta\theta^2}\right)\right]F_{sh}(\theta) \ , \tag{31}$$

where T = 0.21 is the percentage of light that passes through the media without scattering, $\Delta\theta = 45°$ is the full width at half power (FWHP) of the far-field of the laser without a scattering element in vertical direction. $F_{sh}(\theta)$ is a function that accounts for the light blocked (shadowed) by the laser die and the

submount. This function depends on packaging details (including the die to submount solder thickness and the size of the scattering element) and is plotted in Fig. 17 for a typical device.

The far field I(φ) of the entire laser insert in the radial direction is found by combining the far field patterns from 6 facets of 3 lasers:

$$I(\varphi) = \sum_{i=0}^{2} \left[ I_s\left(\tfrac{2}{3}\pi i + \varphi\right) + I_s\left(\tfrac{2}{3}\pi i - \varphi\right) \right] \tag{32}$$

and is plotted in Fig. 18.

The lateral far field produced by a single facet of the laser can again be approximated as a Gaussian (Eq 7) on a pedastal (Eq 6):

$$I_{s\|}(\varphi) = \frac{R}{(R^2 + z^2)^{1.5}} \left\{ \frac{1-T}{\pi} + \frac{T}{\sqrt{2\pi}\Delta\theta_{\|}} \exp\left[ -\frac{\arctan(z/R)^2}{2\Delta\theta_{\|}^2} \right] \right\}, \tag{33}$$

where $\Delta\theta_{\|}$=10° is the full width at half power (FWHP) of the lateral far-field of the laser without a scattering element.

The far field $I_{\|}(\varphi)$ of the entire laser insert in the longitudinal direction (see Fig. 19) is found by combining the far field patterns from 10 lasers:

$$I_{\|}(\varphi) = \sum_{i=1}^{N_l} I_{s\|}\left[ z - \Delta z(i - 0.5) \right] , \tag{34}$$

where Δz = 10 mm is the spacing between the lasers in the laser insert and $N_l$ is the number of the lasers on one side of the laser insert (or one third of the total number of lasers).

Assuming i) the intensity at any point in the far-field is the sum of two adjacent lasers, ii) the maximum intensity is at $\theta_{\|} = 0$, and iii) the minimum intensity is between the lasers, the fringe visibility in the lateral direction becomes:

$$V_{\|} \approx V + (1 - V)\frac{\Delta z^2(\Delta z^2 - 2R^2)}{\Delta z^4 + 8R^4 + 6R^2\Delta z^2} , \tag{35}$$

where $V$=0.5 is the fringe visibility of a single laser with a scattering element (see Eq. (8)).

Equation (35) suggests that $\Delta z$ should be smaller than 1.41R (= 14.1 mm) to achieve a fringe visibility of less than 0.5. The present design satisfies this condition. However if the lateral spacing $\Delta z$ of the lasers is increased, the required value of $V$ can be found from Eq. (35). The analysis in sections 4 and 6 can be applied to design a scattering element with the appropriate value of $V$.

Figure 20 is a comparison between the calculated (Eq.(34)) and measured radiation pattern of the entire laser insert in the longitudinal direction at $R$ = 10 mm. The measurement results were obtained using the laser insert prototype shown in Fig. 21 which is based on the design given in Fig. 2 with scattering elements containing 0.4 μm diameter $TiO_2$ particles. As can be seen from Figs. 20 and 21, the radiated power corresponding to lasers 2 through 7 is reasonably uniform, although there is an ~ 25% variation in the output powers from these individual lasers. Laser 7 has a very low output power compared to the others.

A major source of nonuniformity is a variation in the performance of the semiconductor lasers, which can be greatly reduced with commercially produced lasers. Overall, the scattering elements provide the desired redistribution of light.

## 11. Conclusions

A method for designing and optimizing scattering elements to broaden the far field of semiconductor lasers is presented based on metal, dielectric, and metal-coated (composite) dielectric particles suspended in transparent polymers. An extension of Mie theory from spherical particles to random shaped particles showed a slight improvement in scattering efficiency.

An optimum scattering element design for metallic (silver) particles has a size of 4 μm and a loss of 7% and an optimum design for dielectric (TiO2) particles has a size of 100 μm and a loss of 0.1%.

Scattering elements based on composite particles generally are less efficient than those based on all metal or all dielectric scattering particles. The exception is the use of composite light-transparent dielectric particles made of a low-index outer shell and a high-index core, where slight improvements in the scattering element efficiency of 5 to 10% can be achieved. However, this increased scattering comes

at a cost of using big 0.45-micron particles.

The Mie theory developed for composite metal-coated dielectric spheres provides formulas for designing high absorption nanoparticles, which have many medical applications including tissue heating[22].

A semiconductor laser light delivery system prototype was designed and fabricated. The laser insert used scattering elements with $TiO_2$ scattering particles to achieve uniform illumination. The measured distribution of light intensity agrees reasonably with the calculated results. The main source of nonuniformity in the prototype is due to a variation in the performance of individual lasers.

## References


1. E.S. Nyman and P.H. Hynninen, "Research advances in the use of tetrapyrrolic photosensitizers for photodynamic therapy", J. of Photochem. and Photobiol. B, **73**, 1-28 (2004)
2. T. Dalbasti, S. Cagli, E. Kilinc, N. Oktar and M. Ozsoz, **"**Online electrochemical monitoring of nitric oxide during photodynamic therapy"**,** Nitric Oxide, **7**, 301-305 (2002)
3. A. Ruol, G. Zaninotto, M. Costantini, G. Battaglia, M. Cagol, R. Alfieri, M. Epifani and E. Ancona, "Barrett's esophagus: management of high-grade dysplasia and cancer", J. of Surg. Res., **117**, 44-51 (2004)
4. J. Van den Boogert, R. van Hillegersberg, H.J. van Staveren, et al., "Timing of illumination is essential for effective and safe photodynamic therapy: a study in the normal rat esophagus," in Br J Cancer, **79(5-6)**, 825-30 (1999).
5. S.L. Jacques, "Laser-tissue interactions: photochemical, photothermal, and photomechanical mechanisms," in Surgical Clinics of North America, **72**, 531-558 (1992).
6. Diomed Inc. web site: http://www.diomedinc.com/
7. D.R. Doiron, Jr. Narcisco, L. Hugh and P. Paspa, "Continuous gradient cylindrical diffusion tip for optical fibers and method for using" US Patent Number 5,330,465, (1994)

8. X. Gu, R. C.-H. Tam, “Optical fiber diffuser” US Patent Number 6,398,778, (2002).
9. J.C. Chen, B.D. Swanson “Microminiature illuminator for administering photodynamic therapy” US Patent Number 5,571,152, (1996).
10. A. Rosen, H. Rosen, “Catheter with distally located integrated circuit radiation generator”. US Patent Number 4,998,932, (1991)
11. R.A. Hsi, A. Rosen, C. Rodriguez, “Method and apparatus for catheter phototherapy with dose sensing”. Patent Pending, Docket No. 367, (1999).
12. A. Rosen, H. Rosen, Editors, *New Frontiers in Medical Device Technology* (John Wiley and Sons, pages 95-98).
13. R. Smith, G. Mitchell, “Calculation of complex propagating models in arbitrary, plane layered, complex dielectric structures”, University of Washington, Seattle, WA, EE Technical report No. 206, (1977), http://engr.smu.edu/ee/smuphotonics/Modeig.htm
14. D.P. Bour, R.S. Geels, D.W. Treat, T.L. Paoli, F.Ponce, R.L. Thorton, B.S. Crusor, R.D. Bringans, and D.F. Welch, “Strained $Ga_xIn_{1-x}P/(AlGA)_{0.5}In_{0.5}P$ heterostructures and quantum-well laser diodes”, IEEE J. of Quantum Electronics, **30**, 593-607 (1994).
15. S. T. Flock, S. L. Jacques, B. C. Wilson, et al, “Optical properties of intralipid: A phantom medium for light propagation studies”, Lasers Surg. Med., **12**, 510-9 (1992).
16. H.C. van de Hulst, *Light scattering by small particles*, (John Wiley and Sons, 1964).
17. P. Debye, “The diffraction theory of aberrations,” Ann. Physik, **30**, 59 (1909).
18. *Handbook of optical constants of solids*/ edited by E. D. Palik (Academic Press, 1998).
19. A. K. Fung, *Microwave scattering and emission models and their applications*, (Artech House, 1994).
20. T. Ji, Y. Avny, D. Davidov, “Preparation and optical properties of Au-shell submicron polystyrene particles,” in *Mat. Res. Soc. Symp. Proc.*, Vol 636, (2001).
21. Microfab Technologies Inc. website www.microfab.com
22. L. R. Hirsch, R. J. Stafford, J. A. Bankson, S. R. Sershen, B. Rivera, R. E. Price, J. D. Hazle, N. J. Halas and J. L. West "Nanoshell-mediated near-infrared thermal therapy of tumors under magnetic

resonance guidance," PNAS, **23**, 13549, (2003).

## Figure Captions

Fig.1. A schematic of a balloon catheter (Designed In collaboration with Duane Horton, Mallinckrodt Medical[10-12]);

Fig. 2. Laser insert design a) side view; b) mechanical cross section of laser insert; c) radiation pattern of laser insert; and d) edge-emitting 635nm laser on a Cu submount with a scattering element

Fig.3. Rectangular scattering element with the particles

Fig.4. Scattering intensity function $F(\theta)$ for a silver sphere with $kD = 20$.

Fig. 5. The far field of the laser light that passes without scattering (a), far field of scattered light (b) and total far field of the laser with optical scattering element (c) as a superposition of (a) and (b).

Fig. 6. Uniform scattering and absorption efficiency factors for gold (solid line) and silver (dotted line) spheres

Fig. 7. a) Percentage of light absorbed in the scattering element required to achieve a uniformity of 0.5, for particles of different diameters. b) Size of the scattering element required to achieve a uniformity of 0.5 for particles of different diameters. The host polymer has a refractive index of 1.51 and an absorption coefficient of 5%/cm. The wavelength of the scattered light is 635 nm. The fraction of scattering particles by volume is 1%.

Fig 8. Size of the scattering element required to achieve a uniformity of 0.5 for non-absorbing particles of arbitrary refractive index and various diameters. The host polymer has a refractive index of 1.51 and an absorption coefficient of 5%/cm. The wavelength of the scattered light is 635 nm. The fraction of scattering particles by volume is 1%.

Fig. 9. a) Percentage of light absorbed in the scattering element required to achieve a uniformity of 0.5, for particles in the scattering element with an arbitrary complex index of refraction. b) Size of the scattering element required to achieve a uniformity of 0.5 for particles in the scattering element with an arbitrary complex index of refraction. In both a) and b) the particle diameter is fixed at 0.12 microns, the host polymer has a refractive index of 1.51 and an absorption coefficient of

5%/cm. The wavelength of the scattered light is 635 nm. The fraction of scattering particles by volume is 1%.

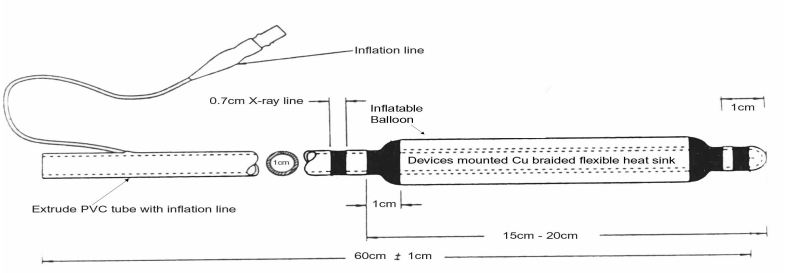


Fig.1. A schematic of a balloon catheter (Designed In collaboration with Duane Horton, Mallinckrodt Medical[10-12]);

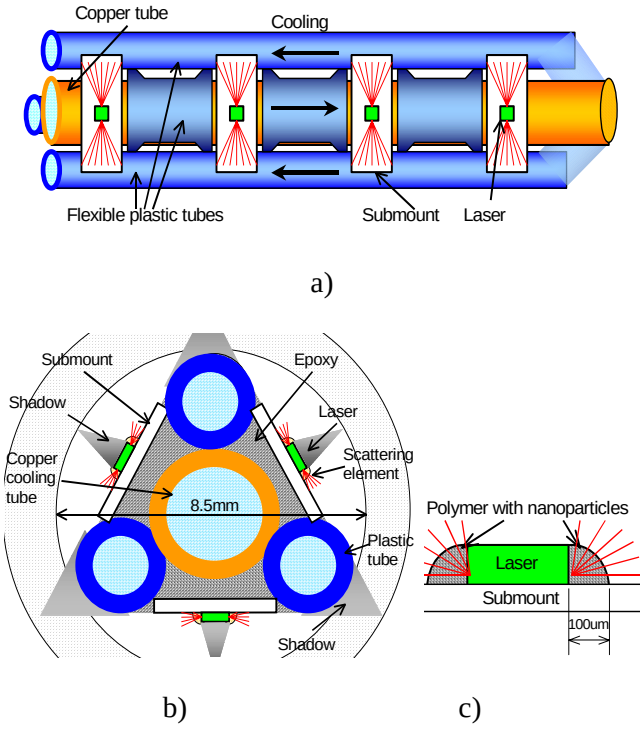


Fig. 2. Laser insert design a) side view; b) mechanical cross section of laser insert; c) radiation pattern of laser insert; and d) edge-emitting 635nm laser on a Cu submount with a scattering element

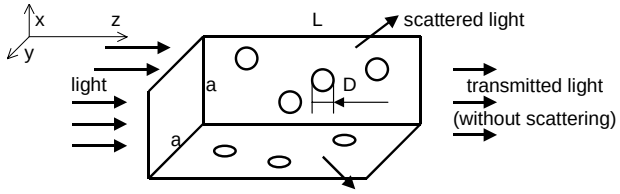


Fig.3. Rectangular scattering element with the particles

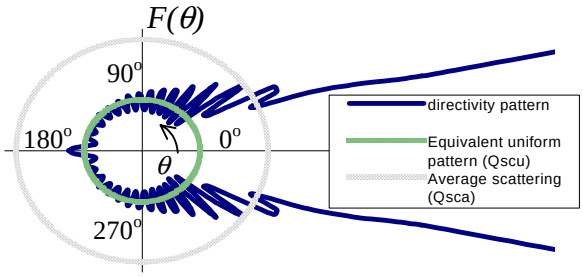


Fig.4. Scattering intensity function $F(\theta)$ for a silver sphere with $kD = 20$.

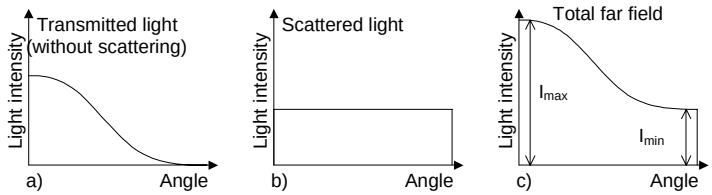


Fig. 5. The far field of the laser light that passes without scattering (a), far field of scattered light (b) and total far field of the laser with optical scattering element (c) as a superposition of (a) and (b).

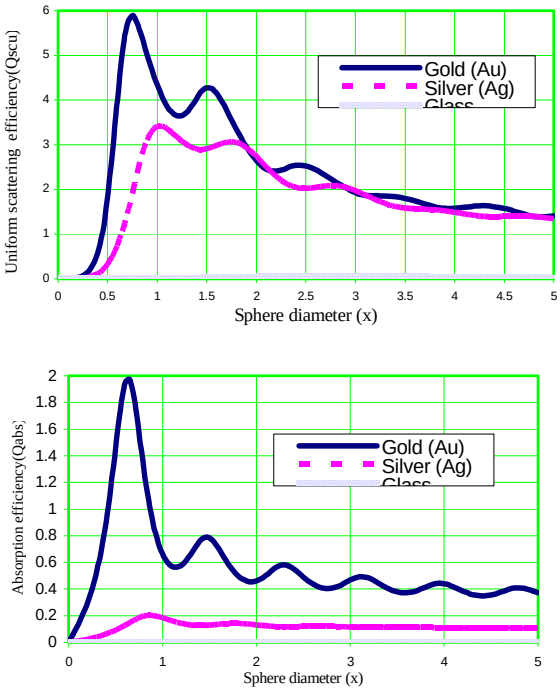


Fig. 6. Uniform scattering and absorption efficiency factors for gold (solid line) and silver (dotted line) spheres

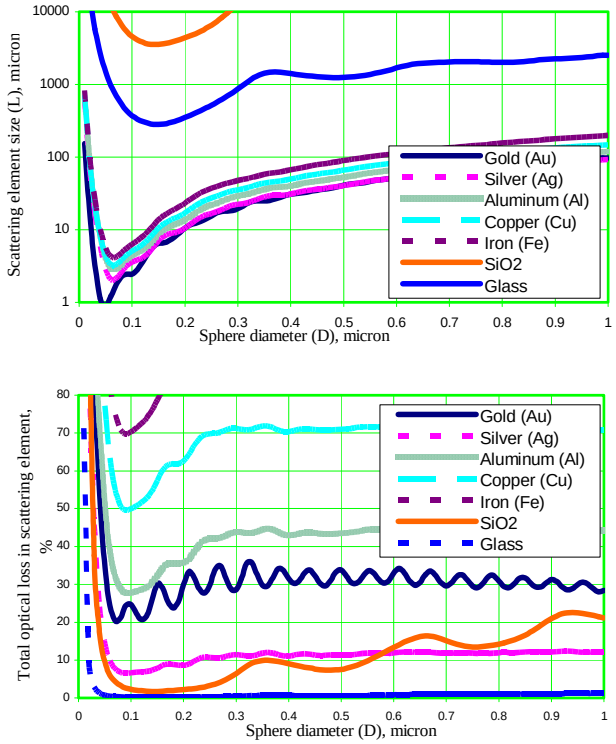


Fig. 7. a) Percentage of light absorbed in the scattering element required to achieve a uniformity of 0.5, for particles of different diameters. b) Size of the scattering element required to achieve a uniformity of 0.5 for particles of different diameters. The host polymer has a refractive index of 1.51 and an absorption coefficient of 5%/cm. The wavelength of the scattered light is 635 nm. The fraction of scattering particles by volume is 1%.

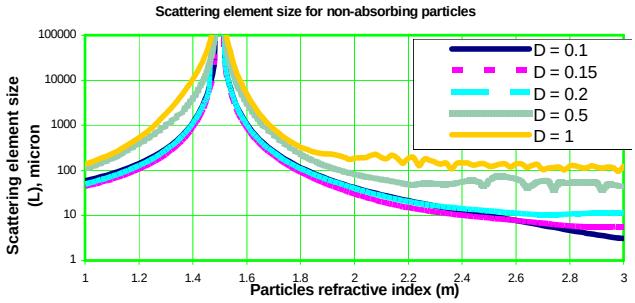


Fig 8. Size of the scattering element required to achieve a uniformity of 0.5 for non-absorbing particles of arbitrary refractive index and various diameters. The host polymer has a refractive index of 1.51 and an absorption coefficient of 5%/cm. The wavelength of the scattered light is 635 nm. The fraction of scattering particles by volume is 1%.

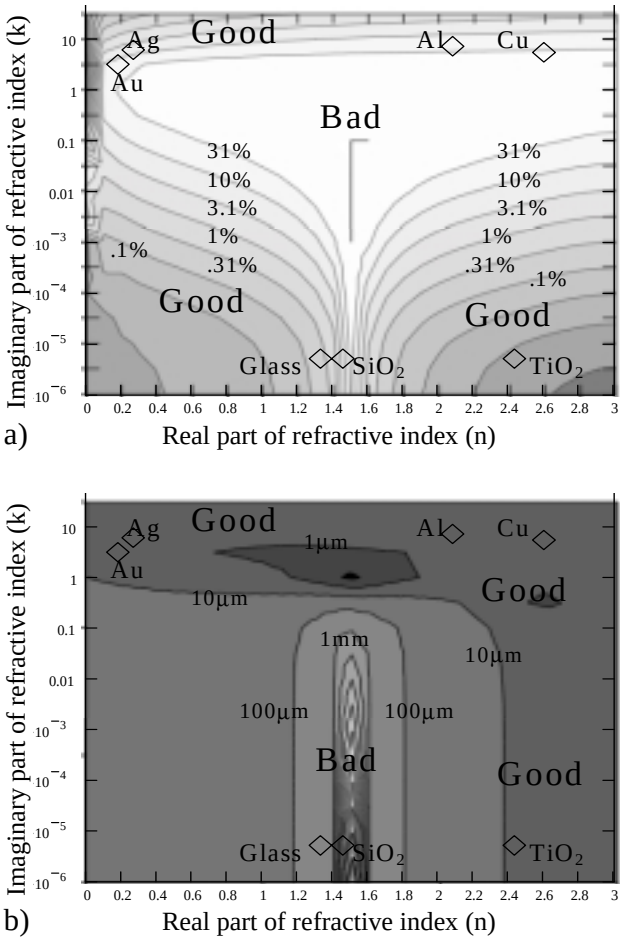


Fig. 9. a) Percentage of light absorbed in the scattering element required to achieve a uniformity of 0.5, for particles in the scattering element with an arbitrary complex index of refraction. b) Size of the scattering element required to achieve a uniformity of 0.5 for particles in the scattering element with an arbitrary complex index of refraction. In both a) and b) the particle diameter is fixed at 0.12 microns, the host polymer has a refractive index of 1.51 and an absorption coefficient of 5%/cm. The wavelength of the scattered light is 635 nm. The fraction of scattering particles by volume is 1%.

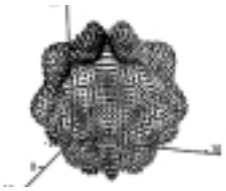

Fig. 10. Particle shape for $K=6$, $\Delta r/r_0=20\%$

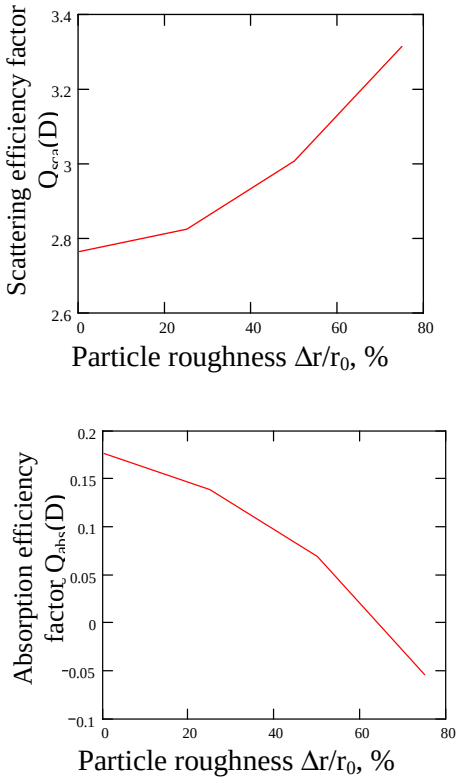


Fig.11. Scattering and absorption efficiency factors for 1 micron gold particles with respect to roughness, $k=6$

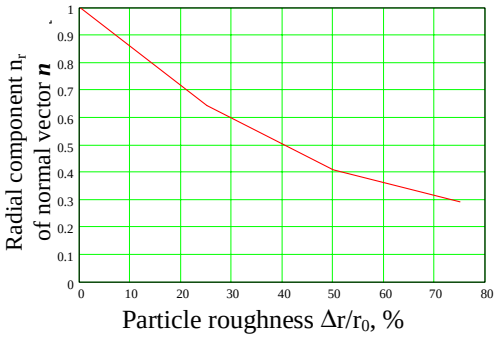


Fig. 12. Radial component $n_r$ of normal vector **n** averaged over particle surface with respect to roughness, *k*=6.

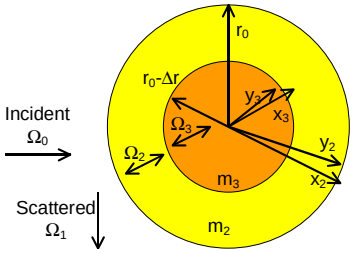


Fig. 13. Composite particle model

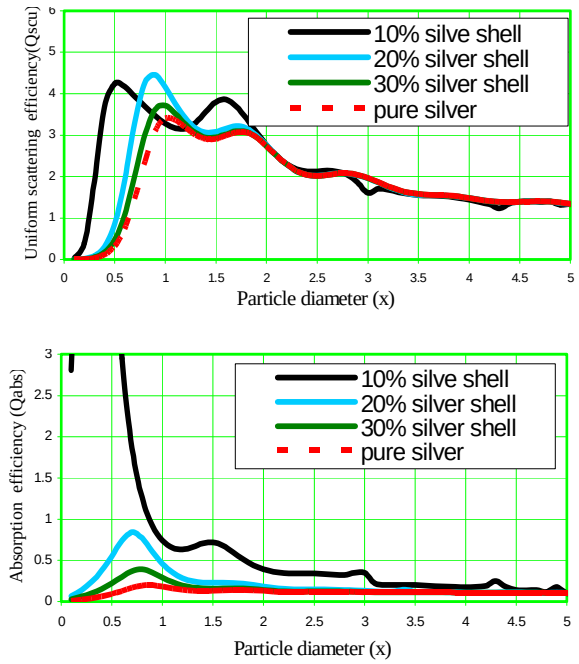


Fig.14. Scattering and absorption efficiency factors as a function of normalized particle diameter for a composite particle with a glass core and a silver shell

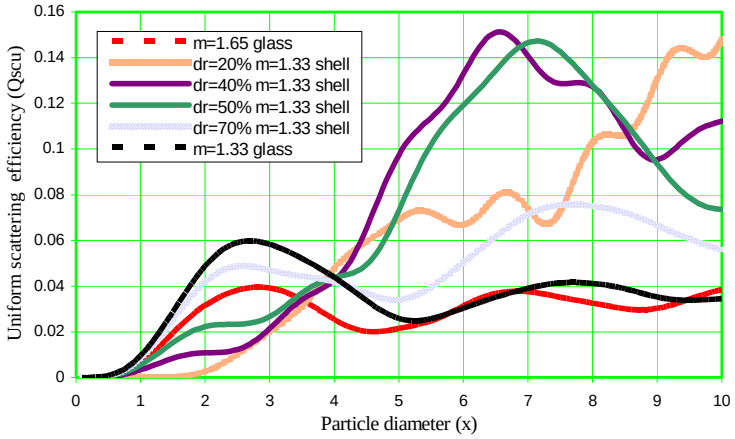


Fig.15. Scattering efficiency factors as a function of normalized particle diameter for a light transparent composite particle with a core refractive index 1.65 and a shell refractive index 1.33.

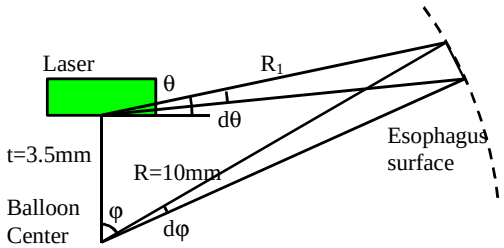


Fig.16. Geometry of the laser insert

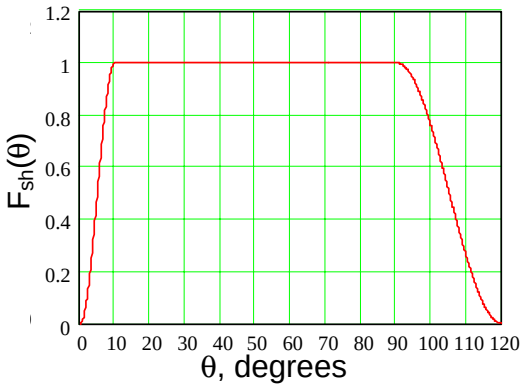


Fig.17. Light blocking function $F_{sh}(\theta)$.

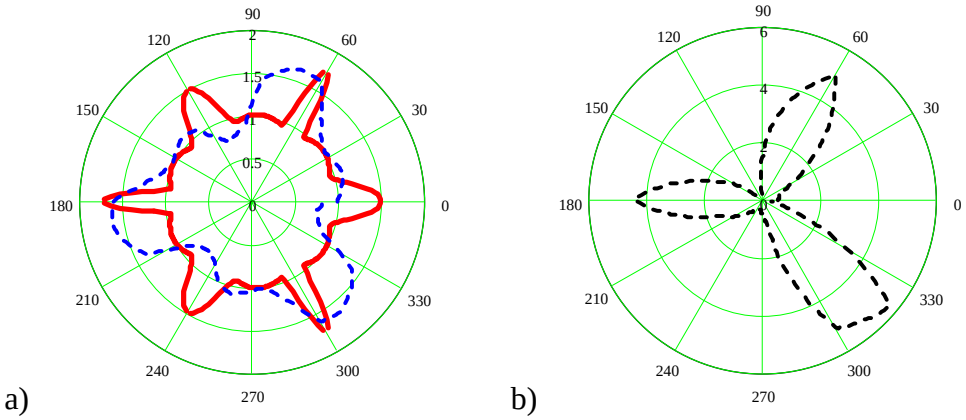


a) b)

Fig.18. a) Calculated (solid line) and measured (dashed line) radial radiation pattern at R = 10 mm.

b) Dashed line represents measured radiation pattern before scattering element deposition.

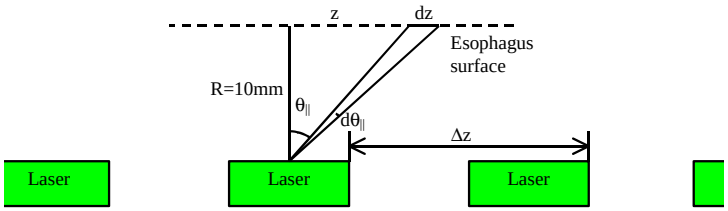


Fig.19. Geometry of the laser insert in the lateral direction

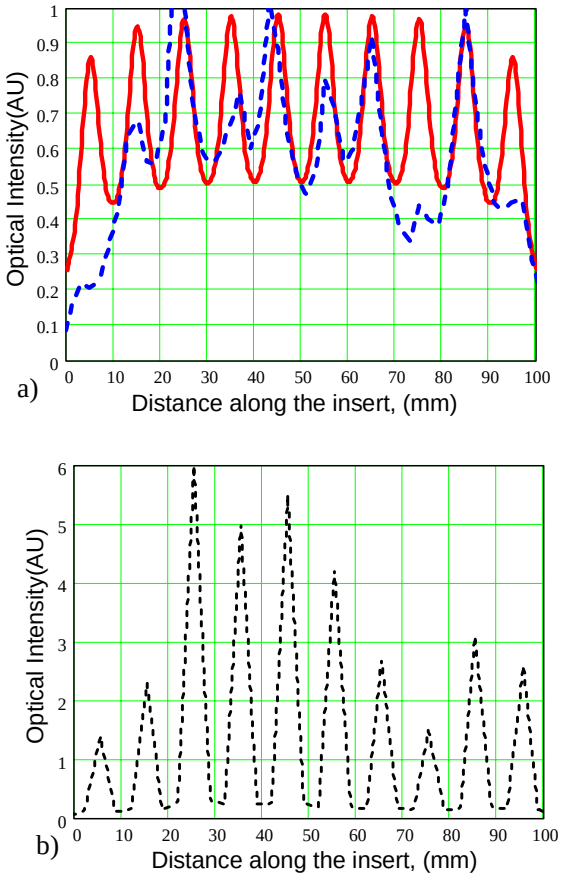


Fig.20. a) Calculated (solid line) and measured (dashed line) lateral radiation pattern at R = 10 mm.

b) Dashed line represents measured radiation pattern before scattering element deposition.

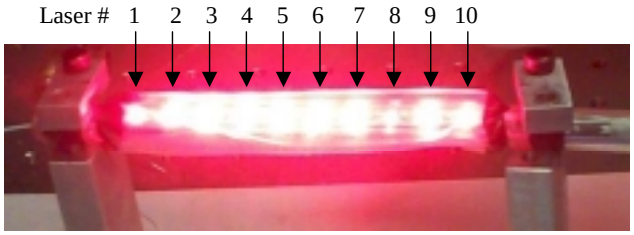


Fig.21. Light delivery system prototype.

Table 1. Calculated results for spheres of optimum diameter

| **Particle Material** | **Refractive index, m** | **Optimal diameter** | **$Q_{ext}$** | **$Q_{sca}$** | **$Q_{scu}$** | **$Q_{abs}$** | **L, μm** | **A, %** |
|---|---|---|---|---|---|---|---|---|
| Au | .180-3.05i | 0.12 | 4.955 | 4.445 | 3.44 | 0.511 | 3.63 | 20.7 |
| Ag | 0.27-5.79i | 0.1 | 3.101 | 2.973 | 2.892 | 0.128 | 3.6 | 6.68 |
| Al | 2.08-7.15i | 0.1 | 2.904 | 2.417 | 2.337 | 0.487 | 4.45 | 27.8 |
| Cu | 2.6-5.26i | 0.1 | 3.108 | 2.201 | 2.046 | 0.907 | 5.08 | 49.9 |
| Fe | 3.12-3.87i | 0.1 | 3.141 | 1.861 | 1.646 | 1.28 | 6.32 | 70.3 |
| $SiO_2$ | 1.46[18] | 0.15 | .0076 | .0076 | .0044 | - | 3541 | 1.77 |
| Glass | 1.33 | 0.15 | 0.092 | 0.092 | 0.055 | - | 282 | 0.14 |